Stem Cell Reports Article



-OPEN ACCESS

Cell networks in the mouse liver during partial hepatectomy

Bin Li,^{1,2,5,*} Daniel Rodrigo-Torres,^{1,2,5,*} Carl Pelz,^{1,2} Brendan Innes,³ Pamela Canaday,¹ Sunghee Chai,^{1,2} Peter Zandstra,⁴ Gary D. Bader,³ and Markus Grompe^{1,2,6,*}

- ¹Oregon Stem Cell Center, Salem, OR, USA
- ²Department of Pediatrics, Papé Family Institute, Oregon Health & Science University, Portland, OR, USA
- ³The Donnelly Centre, University of Toronto, Toronto, ON, Canada
- ⁴Michael Smith Laboratories, University of British Columbia, Vancouver, BC, Canada
- ⁵These authors contributed equally
- ⁶Lead contact

*Correspondence: libin06@gmail.com (B.L.), drodrigo@ed.ac.uk (D.R.-T.), grompem@ohsu.edu (M.G.) https://doi.org/10.1016/j.stemcr.2025.102683

SUMMARY

In solid tissues, homeostasis and post-injury regeneration involve a complex interplay among various cell types. The mammalian liver harbors numerous epithelial and non-epithelial cells, and the global signaling networks governing their interactions are unknown. To unravel the hepatic cell network, we purified 10 different cell populations from normal and regenerative mouse livers. Analyzing their transcriptomes unveiled ligand-receptor interactions and over 50,000 potential cell-cell interactions in both ground state and after partial hepatectomy. Importantly, about half of these differed between the two states, indicating massive changes in the cell network during regeneration. Our study provides the first comprehensive database of potential cell-cell interactions in liver cell homeostasis and regeneration. Leveraging this predictive model, we identified and validated two previously unknown signaling interactions involved in accelerating and delaying liver regeneration. Overall, we provide a novel platform for investigating autocrine/paracrine pathways in tissue regeneration, with broader applications to other complex multicellular systems.

INTRODUCTION

Rodent liver can fully restore itself to its former mass even after 70% partial hepatectomy (PHx), and this system represents a well-studied paradigm in regenerative medicine (Azuma et al., 2007). Hepatocytes, the liver parenchymal cells, quickly proliferate after PHx to replace the liver mass. After PHx, hepatocyte DNA synthesis peaks at 24 h in rats and 36 h in mice (Michalopoulos and DeFrances, 1997). Previous studies have examined the different cell types participating in PHx-induced liver regeneration. For example, liver sinusoidal endothelial cells (LSECs), one of the main cells in the hepatic cell niche, regulate liver regeneration and hepatocyte proliferation (Ding et al., 2010). In addition to LSECs, hepatic stellate cells (HSCs) are also involved in controlling hepatocyte proliferation (Michalopoulos, 2007).

Simultaneously, dividing hepatocytes produce paracrine signaling to activate other non-parenchymal cells (NPCs) (Michalopoulos and DeFrances, 1997) including LSECs, biliary epithelial cells (BECs), and Kupffer cells (KCs). KCs contribute to hepatocyte regeneration via tumor necrosis factor alpha signaling (Shinozuka et al., 1994). While the contribution of individual liver cell types to liver regeneration has been previously examined by looking at their pairwise interactions with hepatocytes (Ding et al., 2010; Huch et al., 2013; Kordes et al., 2014; Li et al., 2017), a global view of all cell-cell interactions (CCInxs) in the adult liver ground state and their changes during regeneration has not been available to date. Importantly, many other cell

types, including cholangiocytes and endothelial cells, also have to divide after PHx to fully restore the tissue. Very little is known about the signaling events that govern the regeneration of non-hepatocytes.

Cells communicate with each other by ligand-receptor interactions via paracrine and autocrine pathways to initiate the responses to PHx. One well-studied example is hepatocyte growth factor (HGF), a ligand secreted by HSC and LSEC, which interacts with the receptor c-Met on hepatocytes to induce hepatocyte proliferation. In rats, plasma HGF increases dramatically 1 h after PHx (Michalopoulos and DeFrances, 1997). HGF overexpression in vivo induces homeostatic hepatocytes to enter the G_0/S phase and mitosis (Michalopoulos, 2007). Although several specific signaling pathways have been analyzed in detail based on a candidate molecule approach, an unbiased method for the identification of all possible signaling events governing liver regeneration has not been available. Given the thousands of potential ligands and receptors in the liver, it is likely that many functionally important signaling pathways remain to be discovered.

Previous reports from the Zandstra lab described the structure and dynamics of the hierarchically organized blood system at the CCInx and intramolecular network levels (Kirouac et al., 2009, 2010). More recently, a significantly improved bioinformatics platform was developed for constructing connectivity-based intercellular signaling networks using the upregulated ligand and receptor genes of different cell types in a tissue (Kirouac et al., 2010). In



Cell type	Surface marker	References.	Biological replicates (Normal)	Biological replicates (PHx 24 h)
BEC	ST14 ⁻ CD26 ⁻ MIC1-1C3 ⁺ CD31CD45 ⁻ CD11b ⁻	Li et al., 2017, Stem Cell Reports	4	2
Blood cell	CD45 ⁺	Alaverdi, 2002, Current Protocols in Immunology	2	2
cBEC	ST14 ⁺ CD26 ⁻ MIC1-1C3 ⁺ CD31CD45 ⁻ CD11b ⁻	Li et al., 2017, Stem Cell Reports	4	2
EC	Lyve1 ⁻ CD34 ⁺ CD144 ⁺ CD309 ⁺ CD45 ⁻	Ding et al., 2010, Nature	2	3
НС	OC2-2F8 ⁺ CD45 ⁻ CD31 ⁻	Huch et al., 2013, Nature	4	4
HSC	CD146 ⁺ CD45 ⁻ CD31 ⁻ Violate ⁺	Mederacke et al., 2015, Nature Protocols	2	3
KC	F4/80 ⁺ CD11b ⁺	Kumar et al., 2006, JCI	2	2
LSEC	Lyve1 ⁺ CD34 ⁻ CD144 ⁺ CD309 ⁺ CD45 ⁻	Ding et al., 2010, Nature	3	5
NPD	CD26 ⁺ MIC1-1C3 ⁺ CD31 ⁻ CD45CD11b ⁻	Dorrell et al., 2011, Gene & Dev	2	2
Thy1	Thy1 ⁺ CD45 ⁻	Hoppo et al., 2004, Hepatology	2	2

HC, hepatocyte.

particular, they explored the intercellular signaling from 11 human bone marrow hematopoietic populations (stem cells, erythroid progenitors, myeloid progenitors, etc.). By integrating high-throughput molecular profiling (transcriptome and proteome), protein interaction and information, and mechanistic modeling with cell culture experiments, they showed that complex intercellular communication networks by secreted factors mediated intercellular communication networks and regulated blood stem cell fate decisions. Several novel unknown ligand/receptor interactions were discovered and validated in HSC expansion cultures in vitro. Here, we adapted this platform to a liver regeneration system to define autocrine and paracrine cell interactions and to predict novel regulators of tissue behavior. We isolated 10 liver cell populations from homeostatic adult mice after induction of liver regeneration by PHx. We performed bulk RNA sequencing (RNA-seq) independently on each population and constructed CCInx (Ximerakis et al., 2019) by matching the ligand and receptor pairs in the ligand-receptor database. A dense map of potential intercellular interactions was identified, and two previously unknown receptor-ligand interactions important for liver regeneration were discovered and functionally validated.

RESULTS

Isolation of liver cells with surface markers

To isolate liver cells, we performed a 2-step collagenase perfusion of C57B/L6 wild-type male mice liver at 8 weeks

in the normal state and 24 h after 70% PHx. Hepatocytes and NPCs were collected and labeled with antibodies according to published papers (Table 1) (Alaverdi, 2002; Ding et al., 2010; Dorrell et al., 2011; Hoppo et al., 2004; Huch et al., 2013; Kumar et al., 2006; Li et al., 2017; Mederacke et al., 2015). Fluorescence-activated cell sorting (FACS) was used to isolate 10 distinct populations of interest: regular BECs (ST14⁻CD26⁻MIC1-1C3⁺CD31⁻CD45⁻ CD11b⁻, n = 4 in homeostasis [Li et al., 2017], n = 2 in PHx), blood cells (CD45⁺, Figure S1A, n = 2 in homeostasis, n = 2 in PHx), Thy1+ (Thy1+CD45-, Figure S1A, n = 2 in homeostasis, n = 2 in PHx) cells, clonogenic BECs $(ST14^{+}CD26^{-}MIC1-1C3^{+}CD31^{-}CD45^{-}CD11b^{-}, n = 4 in$ homeostasis [Li et al., 2017], n = 2 in PHx), endothelial cells (Lyve1 $^-$ CD34 $^+$ CD144 $^+$ CD309 $^+$ CD45 $^-$, Figure S1B, n = 2 in homeostasis, n = 3 in PHx), LSECs (Lyve1⁺CD34⁻ CD144⁺CD309⁺CD45⁻, Figure S1B, n = 3 in homeostasis, n = 5 in PHx), hepatocytes (OC2-2F8⁺CD45⁻CD31⁻, Figure S1C, n = 4 in homeostasis, n = 4 in PHx), HSCs $(CD146^+CD45^-CD31^-Violet^+, Figure S1D, n = 2 in homeo$ stasis, n = 3 in PHx), KCs (F4/80+CD11b+, Figure S1E, n = 2in homeostasis, n = 3 in PHx), and non-progenitor ducts (NPDs) (CD26+MIC1-1C3+CD31-CD45-CD11b-, n = 2 in homeostasis, n = 2 in PHx). At least 10,000 cells were collected for each population to extract bulk RNA.

Transcriptome and cell-cell interaction analysis in mouse liver cells

To compare these populations at the transcriptional level, we extracted RNA from freshly FACS-sorted cells to perform



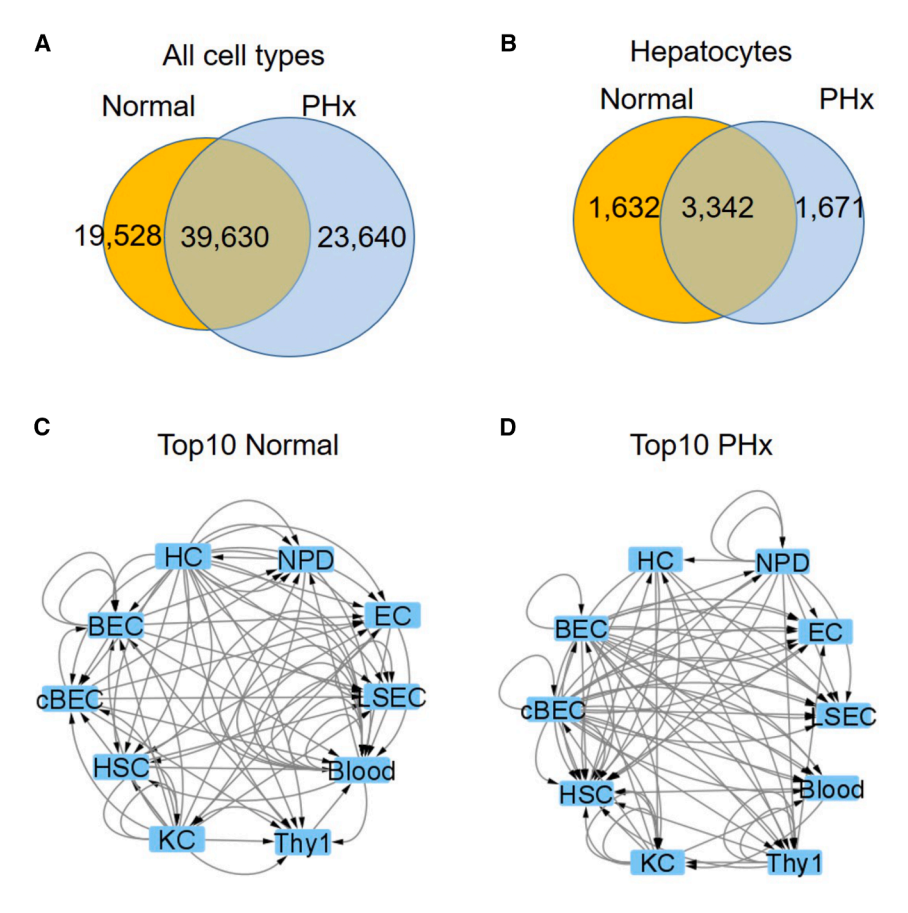


Figure 1. Cell-cell interactions in homeostatic and regenerative liver

(A and B) Venn diagrams of the number of paracrine and autocrine interactions in normal liver and PHx among all 10 cell types (A) and hepatocytes only (B). (A) There are 19,528 unique interactions in normal liver and 23,640 in PHx. The normal and PHx states had 39,630 shared common interactions. (B) In hepatocytes, there were 1,632 unique interactions in normal and 1,671 after PHx, with 3,342 shared common interactions. (C and D) Schematic top 10 CCInx-weighed interactions in normal (C) and PHx (D) livers by Cytoscape network visualization. The interactions are ranked by the edge weights calculated by CCInx. PHx, 24 h after 70% PHx; HC, hepatocyte; blood: blood lineage cells; Thy1, Thy1+ cells. Arrows indicate either autocrine (from one cell to itself) or paracrine (from one cell to another) interactions. See also Figures S1 and S2.

RNA-seq. The data were analyzed using a previously published computer algorithm (Qiao et al., 2014) with a substantially expanded cell interaction database (Ximerakis et al., 2019). In total, we detected 82,978 CCInxs among the 10 isolated cell types. Among them, 39,630 common cell interactions (including autocrine and paracrine pathways) were present in both normal and PHx livers (Figure 1A; Tables S1 and S2). In addition, we identified 19,528 global interactions that were unique to the ground state, whereas there were 23,640 global interactions present only after PHx (Figure 1A; Tables S1 and S2). We next narrowed our analysis to look at only those interactions that involved hepatocytes. Hepatocytes participated in 6,645 interactions, 8.0% of the total (Figure 1B; Tables S1 and S2); 3,342 were present in both homeostasis and the regenerative state. In addition, there were 1,632 unique ground-state interactions (8.4% of global interactions) and 1,671 interactions present only after PHx (7.1% of global interactions) (Figure 1B; Tables S1 and S2). To get a sense of how the cell network changes during regeneration, we looked at the top 10 ranked ligand-receptor interactions (based on CCInx weights calculated using our log2 fold change [FC] calculations for both ligand and receptor) for each cell type in both the normal state

(Figure 1C; Table S3) and after PHx (Figure 1D; Table S4). It is immediately apparent that the network changes between the two states and that input and outputs are different for all cell types. Interestingly, the majority of predicted top interactions occurred between non-hepatocyte populations (Figures 1C and 1D; Tables S3 and S4). Among the top 73 interactions in normal livers, there was only 1 paracrine pathway coming from another cell type (NPD: ligand C3) to hepatocytes (receptor: Cfi) but there were 22 outward paracrine pathways from hepatocytes to other cell types (2 to BEC, 2 to clonal BEC [cBEC], 3 to NPD, 4 to endothelial cells [ECs], 4 to LSEC, 0 to blood, 3 to Thy1, 0 to KC, and 4 to HSC) (Figure 1C; Table S3). In PHx liver, the numbers of signals from hepatocytes to others and others to hepatocytes were 7 (1 to LSEC, 1 to Thy1, 1 to KC, and 4 to HSC) and 3 (HSC: ligand Ecm1, receptor Cfi; NPD: ligand C3, receptor Cfi, Thy1: ligand C3, receptor Cfi), respectively (Figure 1D; Table S4).

Validation of known ligands by CCInx

To determine whether our system could capture transcriptionally regulated receptor-ligand pairs that are known to be important in liver regeneration, we examined such molecules using the previously reported CCInx database



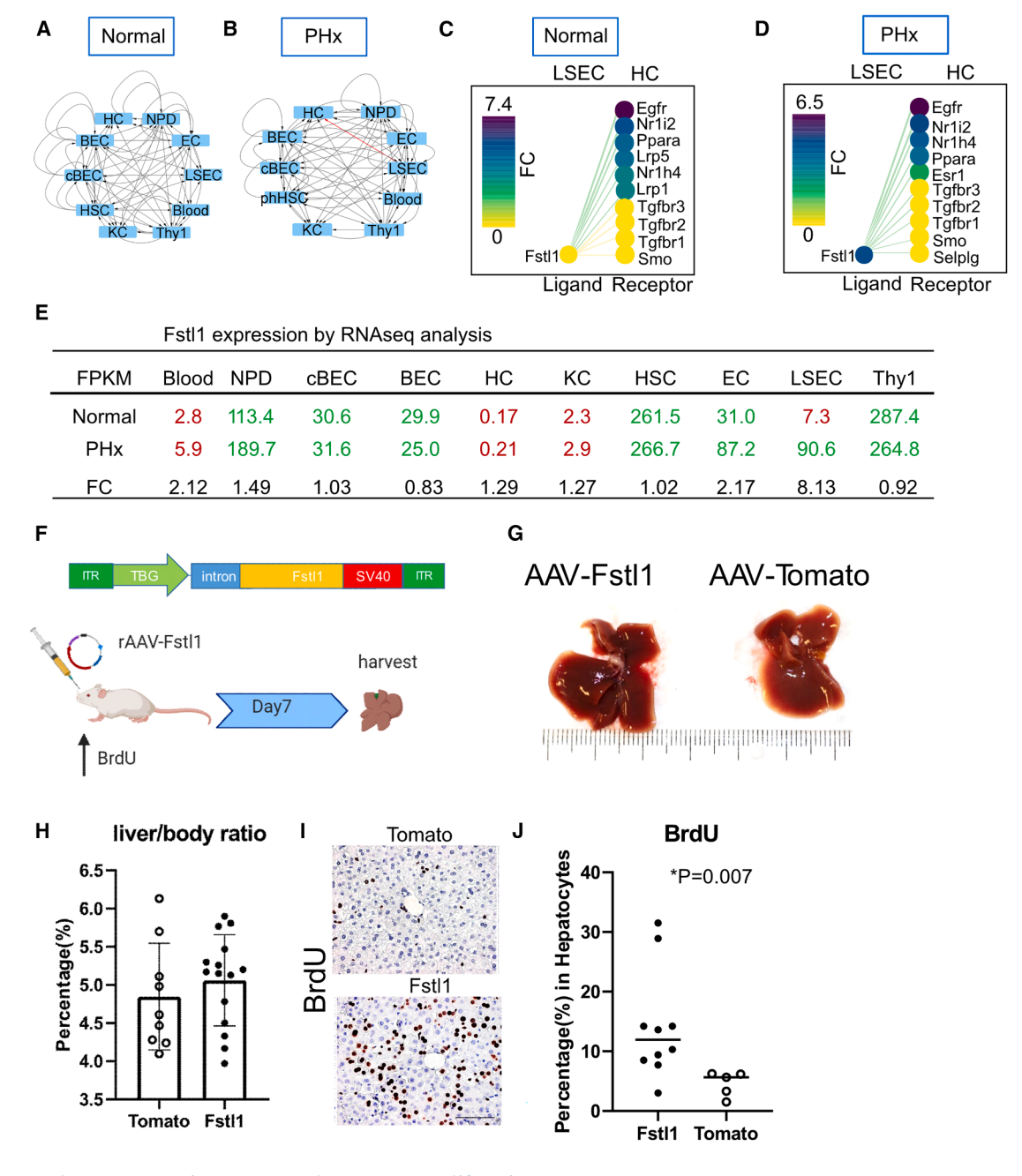


Figure 2. Fstl1 overexpression promotes hepatocyte proliferation

(A and B) Cytoscape network visualization of Fstl1 as a ligand in 10 different cell types from the normal (A) and PHx (B) livers. Arrows indicate the paracrine and autocrine signaling pathways. Red arrow indicates that the paracrine signaling pathway appears in the PHx but not in the normal liver.

(C and D) The CCInx database showed Fstl1 as a ligand in LSEC and its top 10 receptors in HC. Fstl1 is off (yellow circle) (C) in the normal liver but upregulated and on (dark purple circle) after PHx (D).

(E) Normalized gene expression of Fstl1 (tag counts in FPKM) in 10 different cell types from normal liver and PHx. Tag counts in red color, the Fstl1 gene is off; tag counts in green color, the Fstl1 gene is on.

(F) rAAV construct for overexpressing the *Fstl1* gene. The *Fstl1* gene was cloned into an AAV2 vector backbone with the human thyroid hormone-binding globulin (TBG) as promoter. 2×10^{11} vector genomes of AAV-Fstl1 virus were injected into C57BL/6 mice fed with BrdU in the drinking water. The liver was harvested on day 7 after injection.

(legend continued on next page)



(Ximerakis et al., 2019). It has been reported that Pdgfβ and Tgfα induce hepatocyte proliferation in vivo and in vitro, respectively (Li et al., 2022; Mead and Fausto, 1989; Vrochides et al., 1996). Our cell network platform verified that Pdgfß paracrine and autocrine pathways were off in homeostasis (Figure S2A), while they were on after PHx (Figure S2B). We also investigated the Tgf α pathway in homeostasis and PHx in our database (Figures S2C and S2D). As expected, the Tgf α pathway was inactive in LSECs during homeostasis (Figure S2C) but activated after PHx (Figure S2D).

Apart from this validation, we compared our results with previous publications that used a similar approach to identify potential ligand-receptor interactions. Recently, Chembazhi et al., 2021, determined ligand-receptor interactions that occur between cell populations after PHx at 48 h using single-cell RNA sequencing (scRNA-seq) technology. Although the selected time points differed from our analysis (24 h vs. 48 h), we identified representative signals shared in both studies, including some where the ligand is expressed by hepatocytes, such as Vegf2 (receptors Itga9, Itgb1, Kdr, Nrp1, Nrp2, and Flt1), Cxcl2 (receptors Ackr3 and Cd4), and C3 (receptors Lrp1, C3ar1, C3ar2, and CD46). Besides, we identified common signals where the receptor was expressed in hepatocytes such as Met (ligand: Hgf), Il1r1, Il1rap (ligand: Il1a), and Egfr (ligand: Hbegf). However, there are substantial differences as some of the ligands/receptors are not expressed by hepatocytes in our system or the interactions do not occur. These results suggest that some interactions are maintained during an extended period of time during liver regeneration but others are switched off/on as a consequence of the dynamic changes that occur during this process.

Fstl1 as a novel ligand in accelerating liver regeneration

In addition to known pathways, our analysis revealed many previously unexplored receptor-ligand interactions that changed during regeneration and were, therefore, candidates to play a functional role. To probe the predictive value of our network, we performed functional tests on two of these candidates. We mined the data to identify novel candidate ligands that are only present and highly expressed in either homeostasis or perturbation (regenerative liver). A literature review helped us to determine that these molecules had not been previously assessed in the context of liver regeneration. Based on these criteria, we chose the ligands follistatin-like 1 (Fstl1) and secreted frizzled-related protein 1 (Sfrp1) for functional assays. FSTL1 is a secreted glycoprotein that acts as a bone morphogenetic protein 4 (BMP4) antagonist (Geng et al., 2011). Fstl1 interactions from sinusoidal endothelial cells to hepatocytes were off in homeostasis (Figures 2A, 2C, and 2E) but on 24 h after PHx (Figures 2B, 2D, and 2E). In addition, Fstl1 expression in homeostatic LSECs was inactivated but strongly upregulated in PHx (Figure 2E). We then investigated the expression levels of Fstl1 in all different cell types (Figure 2E). Blood cells, hepatocytes, and KCs had low fragments per kilobase per million (FPKM) (<10) before (FPKM = 2.8, 0.17, and 2.3, respectively) and after PHx (FPKM = 5.9, 0.21, and 2.9, respectively), suggesting the gene was completely off in these cells. Bile duct lineage cells (BECs, cBECs, NPD), HSC, and Thy1 populations, had higher levels of Fstl1 but no significant change before and after PHx (Figure 2E). ECs) and LSECs were the only two populations that showed elevated Fstl1 expression after PHx. The physical proximity of LSECs to hepatocytes makes them of particular interest in terms of providing important ligands. Notably, compared to ECs, LSECs had a higher FC (8.16) from homeostasis (FPKM = 11.1) to PHx (FPKM = 90.6), while ECs had a lower increase (FC = 2.17) from homeostasis (FPKM = 40.1) to PHx (FPKM = 87.2).

To test the role of Fstl1 by gain of function in vivo, we constructed self-complementary recombinant adeno-associated virus (AAV) (rAAV) carrying the mouse Fstl1 transgene (Figure 2F) and overexpressed Fstl1 in the liver (Figure S3A). Bromodeoxyuridine (BrdU) was added to the drinking water, and its incorporation into nuclei was used to measure liver cell division over that time period. Seven days after treatment with rAAV-Fstl1, the livers were harvested (Figure 2F). Compared to control mice, in which rAAV carrying the tdTomato transgene was administered, neither the liver size (Figure 2G) nor the liver/body weight ratio changed macroscopically (AAV-Fstl1: 5.1% ± 0.6% vs. AAV-tdTomato: $4.8\% \pm 0.7\%$, Figure 2H).

However, immunohistochemistry showed that after Fstl1 overexpression, >10% of hepatocytes were BrdU+ $(14.1\% \pm 9.2\%, n = 10 \text{ mice, Figures 2I and 2J})$. In contrast, the proportion of BrdU+ hepatocytes in AAV-tdTomato

⁽G) Representative morphology of mouse liver after Fstl1 overexpression. A liver transduced with an AAVDJ-Tomato vector was used as control.

⁽H) Liver-body weight ratio of independent mice treated with AAVDJ-Tomato (n = 9) and AAVDJ-Fstl1 (n = 15). Student's t test. p > 0.05. (I) Histology of anti-BrdU staining in the control (Tomato) and Fstl1 overexpression liver. Scale bar, 50 μm. BrdU-expressing nuclei

⁽J) Percentage of BrdU+ hepatocytes from Fstl1 overexpression (n = 10) and mock (Tomato) (n = 5) transduced mouse liver. Student's t test. *p = 0.007. HC: hepatocytes. See also Figure S3.



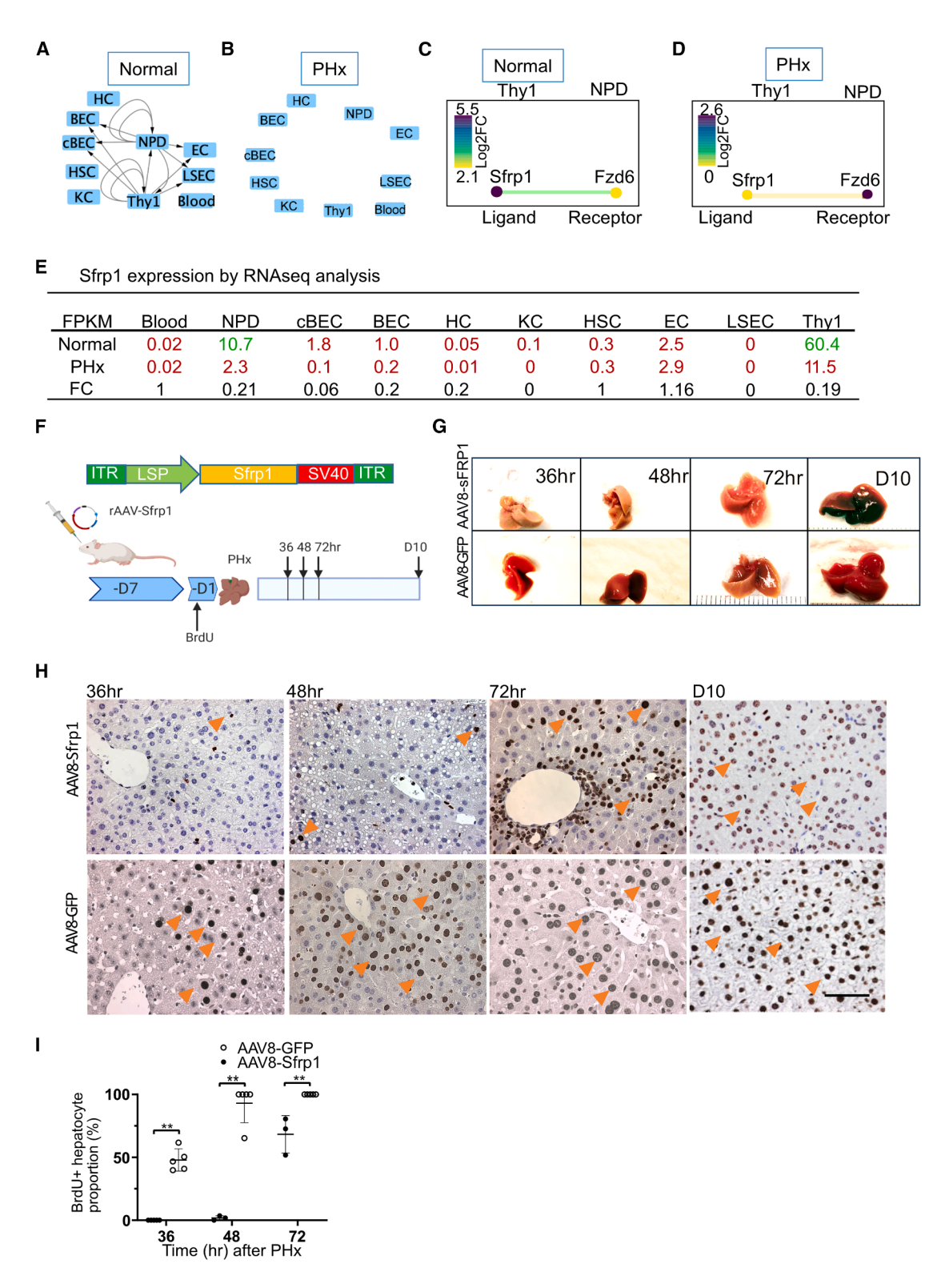


Figure 3. Sfrp1 delays liver regeneration

(A and B) Sfrp1 pathway in 10 different cells in the normal liver (A) and 24 h after 70% PHx (B). Arrows indicate the paracrine and autocrine signaling pathways.

(C and D) Sfrp1 as a ligand in Thy1+ cells and its receptor Fzd6 in NPD.

(legend continued on next page)



control was much lower (4.6% \pm 2.1%, n = 5 mice, *p =0.007, Figure 2J). No hepatic injury was seen by histology. However, when we added recombinant Fstl1 in the hepatocyte culture media, there was no significant hepatocyte proliferation (Figures S3C and S3D). Together, these results show that Fstl1 can powerfully induce hepatocyte replication in vivo but not in vitro.

Sfrp1 as a novel ligand for delaying liver regeneration

Using the same selection criteria, we identified another gene, Sfrp1, which is an antagonist of the Wnt signal pathway. Wnt/β-catenin signals drive PHx-induced liver regeneration (Russell and Monga, 2018). We found that Sfrp1 interactions were active (14 interactions) during mouse liver homeostasis (Figures 3A and 3C) but were quiescent (0 interactions) in the PHx liver (Figures 3B and 3D).

Among the 10 liver cell populations, Sfrp1 was exclusively expressed in Thy1 cells (FPKM >10, Figure 3E). We observed that in the Thy1 population, Sfrp1 expression was significantly downregulated (FC = 0.19) from normal (FPKM = 60.4) to PHx (FPKM = 11.5).

Thus, to evaluate the effects of gain of Sfrp1 function in vivo, we constructed an rAAV carrying an Sfrp1 transgene (Figures 3F and S3B). rAAV-Sfrp1 was administrated 7 days before BrdU administration. One day after BrdU was added to the drinking water, PHx was performed to trigger liver regeneration (Figure 3F). We found that in the Sfrp1 overexpression cohort, the hepatocytes were not marked by BrdU until PHx 48 h, whereas in the control group with rAAV-GFP only, hepatocytes incorporated BrdU as early as 36 h after PHx (Figure 3H). Quantitative analysis demonstrated that after Sfrp1 overexpression, the percentage of BrdU+ hepatocytes was significantly lower than that in the AAV-GFP control at 36, 48 and 72 h after PHx (Figure 3I). These results showed that Sfrp1 is a negative regulator of liver regeneration.

DISCUSSION

Our work described herein provides a first-generation CCInx map based on transcriptome changes during liver regeneration. It is very clear from published work that liver regeneration represents a very complex reorganization of the structure of the entire organ and involves all the many cell types present. Past studies have been largely hepatocyte centric, and much valuable knowledge has been garnered from studying transcriptomic changes in whole liver RNA during regeneration. About 80% of the total RNA in the liver comes from hepatocytes (Li et al., 2017; MacParland et al., 2018), and hence it is easy to detect RNA expression changes in this cell type. However, it is well known that non-hepatocyte liver cells are also very important in initiating and orchestrating liver regeneration (Ding et al., 2010; Huch et al., 2013; Kordes et al., 2014; Li et al., 2017). Genomic studies targeted at specific other cell populations have been published. An example is the wellknown effect of angiocrine factors produced by sinusoidal endothelium (Ding et al., 2010). Based on the understanding that all liver cells have to regenerate to restore liver mass after PHx, we hypothesized that "all cells in the liver talk to all other cells" during the regenerative process. We, therefore, decided to apply the cell interaction network methodology that was successfully applied to the hematopoietic system to the liver. Our analysis provides a comprehensive database of transcriptomic changes in 10 antigenically defined liver cell types. A very rich and dense network of potential interactions was revealed. Indeed, highly significant gene expression changes were observed in all the 10 cell types analyzed, confirming that regeneration requires adaptive changes in all liver-resident cells.

It is important to emphasize that all of the interactions described here in our network represent only potential interactions. Transcriptome data alone do not prove that the ligands and receptors present at the RNA level in different cell types functionally interact. Our network serves to generate hypotheses that need to be validated empirically. Conversely, however, it is relatively safe to assume that interactions involving genes encoding ligands or receptors that are not expressed in a given cell type are, in fact, not active in that cell. Together with information about the expression level of the ligands and receptors as well as literature information, these criteria can be used to prioritize the potential interactions for experimental testing, as we did here.

⁽E) FPKM mapped reads in 10 different cell types from normal liver and PHx. Tag counts in red color, the Sfrp1 gene is off; tag counts in green color, the Sfrp1 gene is on.

⁽F) AAV8-Sfrp1 was transfected into a wild-type mouse 7 days before feeding with BrdU drinking water. One day after BrdU water treatment, PHx was performed. Liver harvest was carried out at 36, 48, 72, and 240 h (day 10) after PHx.

⁽G) Representative morphology of mouse liver overexpressing Sfrp1 with PHx at 36, 48, 72, and 240 h (day10). Liver transfected with AAV8-GFP was used as control.

⁽H) Histology of anti-BrdU staining in the mouse liver treated control (AAV8-GFP) and Sfrp1-overexpressed mouse liver at different time points. Scale bar, 50 µm. BrdU-expressing nuclei stained brown.

⁽I) Quantitative assay of the percentage of BrdU⁺ hepatocytes in the mouse liver treated with control (AAV8-GFP, n = 3) and AAV8-Sfrp1 (n = 5) at different time points. Statistical analyses: Mann-Whitney U test. **p < 0.01. See also Figure S3B.



The analysis of mRNA alone represents a limitation of our method. There are well-known signaling events during liver regeneration (Huh et al., 2004; Ishii et al., 1995; Kaibori et al., 2002; Nejak-Bowen et al., 2013; Patijn et al., 1998) that do not involve changes in the mRNA expression levels of ligands or their receptors. Signaling by HGF, for example, occurs very rapidly without transcriptional activation. Despite this obvious gap in our network, we believe that many important interactions are mirrored at the RNA level and that our network database will be useful to liver biology investigators.

To probe whether our network has any real life validity, we mined the data for yet unpublished CCInxs and performed functional validation experiments with two of these. In both of the examples chosen, our gain-of-function experiments confirmed the activity of the candidate molecules in homeostasis or PHx. We identified Fstl1 as a ligand produced by endothelial cells that significantly induces hepatocyte mitosis. In the heart, FSTL1 has been reported to drive cardiomyocytes to enter the cell cycle in mice (Wei et al., 2015). Recently, it has been shown that engineered FSTL1 patches might help in regenerating adult mammalian myocardium after injury (Hwang et al., 2024). In the liver, FSTL1 has been described to play a role in regulating liver fibrosis and promoting chronic liver disease progression (reviewed in Gu et al., 2023). High levels of circulating FSTL1 have been significantly correlated with improved response in cirrhotic patients (Zheng et al., 2025). In addition, blocking or reducing FSTL1 expression attenuates HSC activation and mitigates liver fibrosis in the CCl₄ injury model (Shang et al., 2017; Xu et al., 2020). However, there is no study assessing its role in liver regeneration. Here, gain of Fstl1 function in vivo also induced hepatocyte division. In addition to Fstl1, we identified Sfrp1 as a negative regulator that delays hepatocyte proliferation after PHx. Sfrp1, a Wnt pathway antagonist, has been reported as an inhibitor of liver cancer cell growth (Shih et al., 2007). Another study showed that Sfrp1 induces retinoblastoma senescence in vitro (Elzi et al., 2012).

Recently, single-cell RNA-seq has been applied for the study of many liver processes and could also be applied to the study of liver regeneration (Halpern et al., 2017; MacParland et al., 2018). Indeed, two papers performed scRNA-seq analysis to also discover novel signals governing regeneration after PHx (Chen et al., 2020; Chembazhi et al, 2021). However, they fail to detect BECs in the analysis; therefore, one of the most prevalent cell types in the liver is not represented in the analysis. In our study, we chose the traditional method of bulk RNA-seq for several reasons. First, genes for ligands and receptors are rarely expressed at high levels and the depth of the transcriptome is shallower with single-cell data, especially for rare popula-

tions (Xiong et al., 2020). Second, we wish to provide a bulk RNA reference including the most representative cell populations in the liver for single-cell data generated by others. It will be interesting to see how well single-cell RNA-seq captures non-abundant transcripts in rare cell populations.

To isolate the different cells of interest, we used FACS sorting technique, which might present some limitations in comparison to scRNA-seq. For example, FACS introduces potential damage to cells, therefore affecting the expression levels of different genes. Besides, it is necessary to have specific markers to isolate pure cell populations; otherwise, one might introduce cell contamination to the different cell types. However, scRNA-seq techniques also have limitations, such as the need of cell annotation for the analysis, the loss of sensitive cells due to the enzymatic digestion, or the alteration of cell proportions (in particular with hepatocytes) (Lin et al., 2024).

In summary, we here provide a first-generation computational model of cell interactions within the mouse liver. Based on this model, we have characterized the contribution of all major cell types participating in the liver regeneration. Functional validation of a small subset of the interactions indicates that this network represents valuable real-life information on how the liver regenerates.

METHODS

Mice

Eight-week-old C57B/L6 male mice were purchased from The Jackson Laboratory. All animal experimentation was conducted in accordance with protocol IP00000445 of the Institutional Review Committee at Oregon Health & Science University. To perform a 70% PHx, the left lobe and median lobes were removed in the morning (Mitchell and Willenbring, 2008). For cell isolation after PHx, livers were perfused 24 h after PHx.

Cell isolation and FACS sorting

To produce single liver cell suspensions for FACS, mouse livers were perfused with 0.5 mM EGTA (Fisher Scientific, O2783) followed by collagenase II (Worthington Biochemical). The isolation of hepatocytes and defined NPC subpopulations from adult mouse liver was performed as previously described (Li et al., 2017, 2019) with some modifications. Briefly, hepatocytes were pelleted at $50 \times g$ for 5 min. The supernatant was then spun down at 1,400 rpm for 5 min to pellet NPCs. Undigested tissue was further digested with collagenase IV (Worthington Biochemical) for 20 min at 37° C with stirring. Digested tissue was filtered with a 40-µm cell strainer to collect NPCs. Leftover tissue was further digested with 0.25% trypsin



(Thermo Fisher Scientific) for another 20 min at 37°C with stirring. All digested mixtures were pooled to collect NPCs. For hepatocyte antibody labeling, cells were incubated at 4°C for 30 min with monoclonal anti OC2-2F8 hybridoma supernatant at a dilution of 1:20 and anti-CD45 at a concentration of 1:100. BEC, cBEC, and NPD antibody labeling was performed as described (Li et al., 2017). Other antibodies used for FACS are listed in Table S5.

Cell culture

To test the effects of FSTL1 in vitro, hepatocytes were freshly isolated from 8-week-old male C57B/L6 mice. Cryopreserved human hepatocytes were purchased from BioIVT. Both human and mouse hepatocytes were plated on collagen I-coated tissue culture plate at a density of 1×10^5 /cm² in Williams' E medium (Thermo Fisher) and 10% FBS (Thermo Fisher). Recombinant mouse follistatinlike 1 protein (rFSTL1; R&D systems, MN, #1738-FN, 100 ng/mL) was added into the culture media 24 h after plating the cells and incubated for 24 h. After 24 h, media was changed back to William'E media and 10% FBS without rFSTL1.

RNA sequencing

Cells were directly sorted into 0.5 mL TRIzol-LS (Thermo Fisher, 10296028) in 1.5-mL tubes (Eppendorf, CT) for RNA extraction. For rare sorted cell populations (<10,000 cells/mouse) multiple mice were perfused to collect and pool RNA. cDNA libraries were made with the Illumina TruSeq 2.0 (Illumina, CA) kit following the manufacturer's instructions. The sequence reads were trimmed to 44 bases and aligned to the mouse genome NCBI37/mm9 using Bowtie (an ultrafast memory-efficient short-read aligner) v. 0.12.7 (Langmead et al., 2009). We used custom scripts to count sequences in exons annotated for RefSeq mouse genes. DESeq2 (Love et al., 2014) was used to calculate the significance of differentially expressed genes based on these counts. We found some degree of Alb mRNA contamination in non-hepatocyte populations. To estimate hepatocyte contamination, we looked at a set of hepatocyte marker genes (Serpina1a, Alb, Trf, Ttr, Hnf4a, Tat, Hpd, F9, Cyp2e1, and Cyp3a11). For each of these genes, we calculated the average abundance in hepatocytes (based on FPKM values). We also calculated the abundance of these genes in each of the non-hepatocyte samples where these genes are not expected to be expressed. Estimated contamination was based on the marker gene with the highest ratio in the test sample compared to the hepatocytes. To correct for this contamination, we calculated the average contribution of each gene in the hepatocytes and then applied the estimated contamination ratio from the sample being adjusted. For each gene, we subtracted this value. Finally, we updated the FPKM values of the

adjusted sample to account for the loss in overall expression level. This process was applied separately for preand post-PHx samples. The RNA-seq FASTQ data were submitted to the NCBI-based platform Gene Expression Omnibus: GSE226004.

CCInx analyses

The algorithm was adapted from previous analyses (Qiao et al., 2014). To find active receptor-ligand interactions, we used the distribution of expression levels in our data to select an on (active) level for each gene. Specifically, we applied a single-factor ANOVA test to each gene with the factor being cell type (pre- and post-PHx were handled separately). For genes with significant (p value < 0.01) changes in expression, we divided into two groups by k-means clustering and defined these as on (higher expression) and off (lower expression) states. For each cell type, we checked to see if a gene is called as on for all replicates and if the average expression of all replicates is at least 2-fold greater than the average expression of all cases of this gene in the off state (averaging is done on log scaled data). If so, this gene is called as on for that cell type. A ligand-receptor interaction is only considered valid when both associated genes are on for the respective cell types. The magnitude of each interaction is based on the average log2 FC of the on states for the respective cell types. However, this log2 FC value is set to 0 for genes that are not called as on. Cell network in Figures 1C, 1D, 2A, 2B, 3A, and 3B were analyzed by Cytoscape (Shannon et al., 2003).

Plasmids

The Fstl1 cDNA clone was purchased from GeneCopoeia Mm02579, NCBI entry NM_008047. To make AAV-Fstl1, a DNA fragment containing the human thyroxine-binding globulin (TBG) promoter (Yan et al., 2012) and Fstl1 transgene were cloned into a self-complementary rAAV vector between two inverted terminal repeats (ITRs). The primers for in-fusion cloning (Takara Bio) Fstl1 are forward: 5'- CA CAGACGCGTACCGGTGCCACCATGTGGAAACGATGGC TGGCGCTC-3', and reverse: 5'-GTGAGGCCTAGCGGCCG CTTAGATCTCTTTGGTGTTCACCTT-3'.

Mouse cDNA was synthesized by reverse transcription from kidney RNA by M-MLV (Thermo Fisher 28025013) with random primers (Invitrogen 48190011). A fulllength Sfrp1 cDNA fragment was obtained by PCR amplifying mouse kidney cDNA using PrimeStar HS DNA polymerase (Takara Bio) following manufacturer's protocol. The primers for Sfrp1 in-fusion cloning (Takara Bio) are forward: 5'-CTAGTGATTTCGCCGCCACCATGGGCGTCGGG CGCAGCGCGCG-3', and reverse: 5'- TCAGGTCAGCT ATCTTACTTGTACAAGCTTCACTTAAAAACAGACTGGAA GGTG-3'.



To make AAV-Sfrp1, the DNA fragment containing a liver-specific promoter1 (LSP1) (a gift from Hiroyuki Nakai lab) and *Sfrp1* transgene was cloned into a self-complementary AAV vector between two ITRs.

Sequences for Fstl1 and Sfrp1 cDNAs and TBG promoter are listed in Table S5.

rAAV production and in vivo administration

Recombinant Fstl1 was packaged into the AAV-DJ capsid (Grimm et al., 2008), and Sfrp1 was produced with serotype AAV8 (Gao et al., 2002). The rAAV vector preparations were made using the standard triple plasmid co-transfection method and purified with iodixanol gradient ultracentrifugation (Zhang et al., 2021). rAAV titers were determined by dot blot hybridization (Zhang et al., 2021). For AAVDJ-Fstl1 administration, 8-week-old male mice obtained from Jackson Laboratory received 2×10^{11} vg of AAVDJ-Fstl1 or AAVDJ-tdTomato (control) vector diluted in saline solution (100 μL total) via retro-orbital injection. For AAV8-Sfrp1 administration, 3- and 8-week-old male mice obtained from Jackson Laboratory received 2×10^{11} vg of AAV8-SFRP1 or AAV8-GFP (control) vector diluted in saline solution (100 µL total) via retro-orbital injection. One week after rAAV injection, mice were subjected to 70% PHx and sacrificed as indicated.

BrdU labeling

BrdU (Thermo Fisher Scientific, H27260) was given in the drinking water (0.5 mg/mL) as indicated. For BrdU histochemistry, the sections were treated with 2N HCl for 1 h and then stained with anti-BrdU (Abcam, ab6326) anti-body (Willenbring et al., 2008).

Statistical analyses

All data are presented as mean \pm SD. GraphPad Prism software was used for statistical analyses. p < 0.05 and p < 0.01 were considered to be statistically significant and highly significant, respectively.

RESOURCE AVAILABILITY

Lead contact

Further information and requests for resources and reagents can be directed to the lead contact, Markus Grompe (grompem@ohsu.edu).

Materials availability

AAV plasmids generated in this manuscript are available upon request to the lead contact.

Data and code availability

The accession number for the RNA-seq data reported in this paper is Gene Expression Omnibus: GSE226004.

ACKNOWLEDGMENTS

AAV plasmids with TBG and LSP1 promoters were generous gifts from the Hiroyuki Nakai lab. This work was supported by NIH grants R01-DK051592 and R01DK083355 to M.G. D.R.-T. was supported by the Alfonso Martín Escudero Foundation Fellowship. The authors thank OHSU core services Massively Parallel Sequencing Shared Resource and OHSU Flow Cytometry Shared Resources. We thank Milton Finegold and Angela Major for histology assistance. We also thank Leslie Wakefield, Geoff Clarke, Shinichiro Ogawa, and Jeffrey Posey for their excellent technical assistances.

AUTHOR CONTRIBUTIONS

M.G. supervised, designed the experiments, and wrote the manuscript. B.L. and D.R.-T. designed and conducted the experiments and wrote the manuscript. C.P. designed and generated the RNA-seq analysis data and adapted CCInx. B.I., P.Z., and G.D.B. generated the cell network platform. S.C. assisted with vector construction. P.C. assisted with the flow cytometry-related experiments.

DECLARATION OF INTERESTS

M.G. is a founder and shareholder of Yecuris. M.G. is a scientific advisor of Cytotheryx, Inc. and NewLimit.

SUPPLEMENTAL INFORMATION

Supplemental information can be found online at https://doi.org/10.1016/j.stemcr.2025.102683.

Received: October 11, 2024 Revised: September 24, 2025 Accepted: September 25, 2025

REFERENCES

Alaverdi, N. (2002). Monoclonal antibodies to mouse cell-surface antigens. Curr. Protoc. Immunol. Appendix *4*, A.4B.1–A.4B.25. https://doi.org/10.1002/0471142735.ima04bs47.

Azuma, H., Paulk, N., Ranade, A., Dorrell, C., Al-Dhalimy, M., Ellis, E., Strom, S., Kay, M.A., Finegold, M., and Grompe, M. (2007). Robust expansion of human hepatocytes in Fah-/-/Rag2-/-/Il2rg-/- mice. Nat. Biotechnol. *25*, 903–910. https://doi.org/10.1038/nbt1326.

Chembazhi, U.V., Bangru, S., Hernaez, M., and Kalsotra, A. (2021). Cellular plasticity balances the metabolic and proliferation dynamics of a regenerating liver. Genome Res *31*, 576–591. https://doi.org/10.1101/gr.267013.120.

Chen, T., Oh, S., Gregory, S., Shen, X., and Diehl, A.M. (2020). Single-cell omics analysis reveals functional diversification of hepatocytes during liver regeneration. JCI. Insight *5*, e141024. https://doi.org/10.1172/jci.insight.141024.

Ding, B.-S., Nolan, D.J., Butler, J.M., James, D., Babazadeh, A.O., Rosenwaks, Z., Mittal, V., Kobayashi, H., Shido, K., Lyden, D., et al. (2010). Inductive angiocrine signals from sinusoidal



endothelium are required for liver regeneration. Nature 468, 310-315. https://doi.org/10.1038/nature09493.

Dorrell, C., Erker, L., Schug, J., Kopp, J.L., Canaday, P.S., Fox, A.J., Smirnova, O., Duncan, A.W., Finegold, M.J., Sander, M., et al. (2011). Prospective isolation of a bipotential clonogenic liver progenitor cell in adult mice. Genes Dev 25, 1193-1203. https://doi. org/10.1101/gad.2029411.

Elzi, D.J., Song, M., Hakala, K., Weintraub, S.T., and Shiio, Y. (2012). Wnt antagonist SFRP1 functions as a secreted mediator of senescence. Mol. Cell Biol. 32, 4388-4399. https://doi.org/10.1128/ MCB.06023-11.

Gao, G.P., Alvira, M.R., Wang, L., Calcedo, R., Johnston, J., and Wilson, J.M. (2002). Novel adenoassociated viruses from rhesus monkeys as vectors for human gene therapy. Proc. Natl. Acad. Sci. USA 99, 11854–11859. https://doi.org/10.1073/pnas.182412299.

Geng, Y., Dong, Y., Yu, M., Zhang, L., Yan, X., Sun, J., Qiao, L., Geng, H., Nakajima, M., Furuichi, T., et al. (2011). Follistatin-like 1 (Fstl1) is a bone morphogenetic protein (BMP) 4 signaling antagonist in controlling mouse lung development. Proc. Natl. Acad. Sci. USA 108, 7058-7063. https://doi.org/10.1073/pnas.1007293108.

Grimm, D., Lee, J.S., Wang, L., Desai, T., Akache, B., Storm, T.A., and Kay, M.A. (2008). In vitro and in vivo gene therapy vector evolution via multispecies interbreeding and retargeting of adenoassociated viruses. J. Virol. 82, 5887-5911. https://doi.org/10. 1128/JVI.00254-08.

Gu, C., Xue, H., Yang, X., Nie, Y., and Qian, X. (2023). Role of follistatin-like protein 1 in liver diseases. Exp. Biol. Med. 248, 193-200. https://doi.org/10.1177/15353702221142604.

Halpern, K.B., Shenhav, R., Matcovitch-Natan, O., Toth, B., Lemze, D., Golan, M., Massasa, E.E., Baydatch, S., Landen, S., Moor, A.E., et al. (2017). Single-cell spatial reconstruction reveals global division of labour in the mammalian liver. Nature 542, 352-356. https://doi.org/10.1038/nature21065.

Hoppo, T., Fujii, H., Hirose, T., Yasuchika, K., Azuma, H., Baba, S., Naito, M., Machimoto, T., and Ikai, I. (2004). Thy1-positive mesenchymal cells promote the maturation of CD49f-positive hepatic progenitor cells in the mouse fetal liver. Hepatology 39, 1362-1370. https://doi.org/10.1002/hep.20180.

Huch, M., Dorrell, C., Boj, S.F., Van Es, J.H., Li, V.S.W., Van De Wetering, M., Sato, T., Hamer, K., Sasaki, N., Finegold, M.J., et al. (2013). In vitro expansion of single Lgr5+ liver stem cells induced by Wnt-driven regeneration. Nature 494, 247-250. https://doi. org/10.1038/nature11826.

Huh, C.G., Factor, V.M., Sánchez, A., Uchida, K., Conner, E.A., and Thorgeirsson, S.S. (2004). Hepatocyte growth factor/c-met signaling pathway is required for efficient liver regeneration and repair. Proc. Natl. Acad. Sci. USA 101, 4477-4482. https://doi. org/10.1073/pnas.0306068101.

Hwang, B., Korsnick, L., Shen, M., Jin, L., Singh, Y., Abdalla, M., Bauser-Heaton, H., and Serpooshan, V. (2024). FSTL-1 loaded 3D bioprinted vascular patch regenerates the ischemic heart. tissue.iScience 27, 110770. https://doi.org/10.1016/j.isci.2024.110770.

Ishii, T., Sato, M., Sudo, K., Suzuki, M., Nakai, H., Hishida, T., Niwa, T., Umezu, K., and Yuasa, S. (1995). Hepatocyte growth factor stimulates liver regeneration and elevates blood protein level in normal and partially hepatectomized rats. J. Biochem. 117, 1105-1112. https://doi.org/10.1093/oxfordjournals.jbchem.a124814.

Kaibori, M., Inoue, T., Oda, M., Naka, D., Kawaguchi, T., Kitamura, N., Miyazawa, K., Kwon, A.H., Kamiyama, Y., and Okumura, T. (2002). Exogenously administered HGF activator augments liver regeneration through the production of biologically active HGF. Biochem. Biophys. Res. Commun. 290, 475-481. https://doi.org/ 10.1006/bbrc.2001.6170.

Kirouac, D.C., Ito, C., Csaszar, E., Roch, A., Yu, M., Sykes, E.A., Bader, G.D., and Zandstra, P.W. (2010). Dynamic interaction networks in a hierarchically organized tissue. Mol. Syst. Biol. 6, 417. https://doi.org/10.1038/msb.2010.71.

Kirouac, D.C., Madlambayan, G.J., Yu, M., Sykes, E.A., Ito, C., and Zandstra, P.W. (2009). Cell-cell interaction networks regulate blood stem and progenitor cell fate. Mol. Syst. Biol. 5, 293. https://doi.org/10.1038/msb.2009.49.

Kordes, C., Sawitza, I., Götze, S., Herebian, D., and Häussinger, D. (2014). Hepatic stellate cells contribute to progenitor cells and liver regeneration. J. Clin. Investig. 124, 5503-5515. https://doi.org/10. 1172/JCI74119.

Kumar, V., Ali, S.R., Konrad, S., Zwirner, J., Verbeek, J.S., Schmidt, R. E., and Gessner, J.E. (2006). Cellderived anaphylatoxins as key mediators of antibody-dependent type II autoimmunity in mice. J. Clin. Investig. 116, 512-520. https://doi.org/10.1172/JCI25536.

Langmead, B., Trapnell, C., Pop, M., and Salzberg, S.L. (2009). Ultrafast and memory-efficient alignment of short DNA sequences to the human genome. Genome Biol 10, R25. https://doi.org/10. 1186/gb-2009-10-3-r25.

Li, B., Dorrell, C., Canaday, P.S., Pelz, C., Haft, A., Finegold, M., and Grompe, M. (2017). Adult mouse liver contains two distinct populations of cholangiocytes. Stem Cell Rep 9, 478–489. https://doi. org/10.1016/j.stemcr.2017.06.003.

Li, B., Dorrell, C., Canady, P.S., and Wakefield, L. (2019). Identification and isolation of clonogenic cholangiocyte in mouse. Methods Mol Biol 1905, 19-27. https://doi.org/10.1007/978-1-4939-8961-4_3.

Li, Y., Fan, W., Link, F., Wang, S., and Dooley, S. (2022). Transforming growth factor beta latency: A mechanism of cytokine storage and signalling regulation in liver homeostasis and disease. JHEP Rep 4, 100397. https://doi.org/10.1016/j.jhepr.2021.100397.

Lin, P., Yan, X., Jing, S., Wu, Y., Shan, Y., Guo, W., Gu, J., Li, Y., Zhang, H., and Li, H. (2024). Single-cell and spatially resolved transcriptomics for liver biology. Hepatology 80, 698–720. https://doi. org/10.1097/HEP.0000000000000387.

Love, M.I., Huber, W., and Anders, S. (2014). Moderated estimation of fold change and dispersion for RNA-seq data with DESeq2. Genome Biol 15, 550. https://doi.org/10.1186/s13059-014-0550-8.

MacParland, S.A., Liu, J.C., Ma, X.-Z., Innes, B.T., Bartczak, A.M., Gage, B.K., Manuel, J., Khuu, N., Echeverri, J., Linares, I., et al. (2018). Single cell RNA sequencing of human liver reveals distinct intrahepatic macrophage populations. Nat. Commun. 9, 4383. https://doi.org/10.1038/s41467-018-06318-7.

Mead, J.E., and Fausto, N. (1989). Transforming growth factor alpha may be a physiological regulator of liver regeneration by



means of an autocrine mechanism. Proc. Natl. Acad. Sci. USA *86*, 1558–1562. https://doi.org/10.1073/pnas.86.5.1558.

Mederacke, I., Dapito, D.H., Affò, S., Uchinami, H., and Schwabe, R.F. (2015). High-yield and high-purity isolation of hepatic stellate cells from normal and fibrotic mouse livers. Nat. Protoc. *10*, 305–315. https://doi.org/10.1038/nprot.2015.017.

Michalopoulos, G.K. (2007). Liver regeneration. J. Cell. Physiol. *213*, 286–300. https://doi.org/10.1002/jcp.21172.

Michalopoulos, G.K., and DeFrances, M.C. (1997). Liver regeneration. Science *276*, 60–66. https://doi.org/10.1126/science.276. 5309.60.

Mitchell, C., and Willenbring, H. (2008). A reproducible and well-tolerated method for 2/3 partial hepatectomy in mice. Nat. Protoc. *3*, 1167–1170. https://doi.org/10.1038/nprot.2008.80.

Nejak-Bowen, K., Orr, A., Bowen, W.C., Jr., and Michalopoulos, G. K. (2013). Conditional genetic elimination of hepatocyte growth factor in mice compromises liver regeneration after partial hepatectomy. PLoS One *8*, e59836. https://doi.org/10.1371/journal.pone.0059836.

Patijn, G.A., Lieber, A., Schowalter, D.B., Schwall, R., and Kay, M.A. (1998). Hepatocyte growth factor induces hepatocyte proliferation *in vivo* and allows for efficient retroviral-mediated gene transfer in mice. Hepatology *28*, 707–716. https://doi.org/10.1002/hep. 510280317.

Qiao, W., Wang, W., Laurenti, E., Turinsky, A.L., Wodak, S.J., Bader, G.D., Dick, J.E., and Zandstra, P.W. (2014). Intercellular network structure and regulatory motifs in the human hematopoietic system. Mol. Syst. Biol. *10*, 741. https://doi.org/10.15252/msb. 20145141.

Russell, J.O., and Monga, S.P. (2018). Wnt/ β -catenin signaling in liver development, homeostasis, and pathobiology. Annu. Rev. Pathol. *13*, 351–378. https://doi.org/10.1146/annurev-pathol-020117-044010.

Shang, H., Liu, X., and Guo, H. (2017). Knockdown of Fstl1 attenuates hepatic stellate cell activation through the TGF-beta1/Smad3 signaling pathway. Mol. Med. Rep. *16*, 7119–7123. https://doi.org/10.3892/mmr.2017.7445.

Shannon, P., Markiel, A., Ozier, O., Baliga, N.S., Wang, J.T., Ramage, D., Amin, N., Schwikowski, B., and Ideker, T. (2003). Cytoscape: a software environment for integrated models of biomolecular interaction networks. Genome Res *13*, 2498–2504. https://doi.org/10.1101/gr.1239303.

Shih, Y.L., Hsieh, C.B., Lai, H.C., Yan, M.D., Hsieh, T.Y., Chao, Y.C., and Lin, Y.W. (2007). SFRP1 suppressed hepatoma cells growth through Wnt canonical signaling pathway. Int. J. Cancer *121*, 1028–1035. https://doi.org/10.1002/ijc.22750.

Shinozuka, H., Kubo, Y., Katyal, S.L., Coni, P., Ledda-Columbano, G.M., Columbano, A., and Nakamura, T. (1994). Roles of growth factors and of tumor necrosis factor-alpha on liver cell proliferation induced in rats by lead nitrate. Laboratory investigation; a journal of technical methods and pathology *71*, 35–41.

Vrochides, D., Papanikolaou, V., Pertoft, H., Antoniades, A.A., and Heldin, P. (1996). Biosynthesis and degradation of hyaluronan by nonparenchymal liver cells during liver regeneration. Hepatology 23, 1650–1655. https://doi.org/10.1002/hep.510230648.

Wei, K., Serpooshan, V., Hurtado, C., Diez-Cuñado, M., Zhao, M., Maruyama, S., Zhu, W., Fajardo, G., Noseda, M., Nakamura, K., et al. (2015). Epicardial FSTL1 reconstitution regenerates the adult mammalian heart. Nature *525*, 479–485. https://doi.org/10.1038/nature15372.

Willenbring, H., Sharma, A.D., Vogel, A., Lee, A.Y., Rothfuss, A., Wang, Z., Finegold, M., and Grompe, M. (2008). Loss of p21 permits carcinogenesis from chronically damaged liver and kidney epithelial cells despite unchecked apoptosis. Cancer Cell *14*, 59–67. https://doi.org/10.1016/j.ccr.2008.05.004.

Ximerakis, M., Lipnick, S.L., Innes, B.T., Simmons, S.K., Adiconis, X., Dionne, D., Mayweather, B.A., Nguyen, L., Niziolek, Z., Ozek, C., et al. (2019). Single-cell transcriptomic profiling of the aging mouse brain. Nat. Neurosci. *22*, 1696–1708. https://doi.org/10.1038/s41593-019-0491-3.

Xiong, X., Kuang, H., Liu, T., and Lin, J.D. (2020). A Single-Cell Perspective of the Mammalian Liver in Health and Disease. Hepatology *71*, 1467–1473. https://doi.org/10.1002/hep.31149.

Xu, X.Y., Du, Y., Liu, X., Ren, Y., Dong, Y., Xu, H.Y., Shi, J.S., Jiang, D., Xu, X., Li, L., et al. (2020). Targeting Follistatin like 1 ameliorates liver fibrosis induced by carbon tetrachloride through TGF-beta1-miR29a in mice. Cell Commun. Signal. *18*, 151. https://doi.org/10.1186/s12964-020-00610-0.

Yan, Z., Yan, H., and Ou, H. (2012). Human thyroxine binding globulin (TBG) promoter directs efficient and sustaining transgene expression in liver-specific pattern. Gene *506*, 289–294. https://doi.org/10.1016/j.gene.2012.07.009.

Zhang, Q.-S., Tiyaboonchai, A., Nygaard, S., Baradar, K., Major, A., Balaji, N., and Grompe, M. (2021). Induced liver regeneration enhances CRISPR/Cas9-mediated gene repair in tyrosinemia type 1. Hum. Gene Ther. *32*, 294–301. https://doi.org/10.1089/hum. 2020.042.

Zheng, X., Tian, S., Li, T., Zhang, S., Zhou, X., Liu, Y., Su, R., Zhang, M., Li, B., Qi, C., et al. (2025). Host FSTL1 defines the impact of stem cell therapy on liver fibrosis by potentiating the early recruitment of inflammatory macrophages. Signal Transduct Target. Ther 10, 81. https://doi.org/10.1038/s41392-025-02162-6.